Journal of Hydrology 519 (2014) 399–413

Contents lists available at ScienceDirect

Journal of Hydrology

journal homepage: www.elsevier.com/locate/jhydrol

Conceptualization of a fresh groundwater lens influenced by climate change: A modeling study of an arid-region island in the Persian Gulf, Iran

Davood Mahmoodzadeh [a], Hamed Ketabchi [a,*], Behzad Ataie-Ashtiani [a,b], Craig T. Simmons [b]

[a] Department of Civil Engineering, Sharif University of Technology, PO Box 11155-9313, Tehran, Iran
[b] National Centre for Groundwater Research and Training and School of the Environment, Flinders University, GPO Box 2100, Adelaide, SA 5001, Australia

ARTICLE INFO

Article history:
Received 29 April 2014
Received in revised form 18 June 2014
Accepted 8 July 2014
Available online 18 July 2014
This manuscript was handled by G. Syme, Editor-in-Chief

Keywords:
Climate change
Conceptual aspects
Numerical modeling
The Persian Gulf
Seawater intrusion
Small islands

SUMMARY

Understanding the fresh groundwater lens (FGL) behavior and potential threat of climatic-induced seawater intrusion (SWI) are significant for the future water resources management of many small islands. In this paper, the FGL of Kish Island, an arid-region case in the Persian Gulf, Iran, is modeled using two-dimensional (2D) and three-dimensional (3D) simulations. These simulations are based on the application of SUTRA, a density-dependent groundwater numerical model. Also, the numerical model parameters are calibrated using PEST, an automated parameter estimation code.

Firstly a detailed conceptualization of the FGL model is completed to understand the sensitivity of the FGL to some particular aspects of the model prior to analysis of climate change simulations. For these investigations, the FGL system is defined based on Kish Island system to accomplish the integrated comparison of features of a conceptual model that are representative of real-world systems. This is the first study which adopts such an approach. The comparison of cross-sectional simulations suggests that the two-layer properties of the Kish Island aquifer have a significant influence on the FGL while the impacts of lateral-boundary irregularities are negligible. The impacts of sea-level rise (SLR), associated land-surface inundation (LSI), and variations in recharge rate on the FGL salinization of Kish Island are investigated numerically. Variations of SLR value (1–4 m) and net recharge rate (17–24 mm/year) are considered to cover a possible range of climatic scenarios in this arid-region island. The 2D and 3D simulation results demonstrate that LSI caused by SLR and recharge rate variation impacts are more important factors in the FGL in comparison to estimated SLR impacts without LSI. It is also shown that climate change impacts on the FGL are long-term to reach a new FGL equilibrium in the case of Kish Island's aquifer system. The comparative analysis of 2D and 3D results shows that three-dimensionality is a significant factor, especially in large-scale 3D systems of small islands. The results of this study are expected to have implications for the understanding and management of the fresh groundwater resources of Kish Island and are also expected to be relevant to the study of the impact of climate change on groundwater resources on islands worldwide.

1. Introduction

Small islands, typically identified to be less than 2000 km^2 in areal extent, have particular physical features and unique and delicately balanced hydrological systems. Groundwater in small islands occurs as fresh groundwater lenses (FGLs), a relatively thin layer of freshwater overlying seawater as a result of recharge. FGL salinization caused by seawater intrusion (SWI) has a great impact on groundwater quality and it can prevent FGL utilization (Falkland, 1991; White and Falkland, 2010).

Climate change is one potentially significant factor that is expected to play a role in SWI status. The Intergovernmental Panel on Climate Change (IPCC, 2013) assessment report identifies the small island states as being the most vulnerable areas of the world to the adverse impacts of climate change including sea level rise (SLR), and recharge rate variations. SLR of between 0.26 and 1.8 m could be expected by the end of the 21st century (e.g., Melloul and Collin, 2006; IPCC, 2013; Vermeer and Rahmstorf, 2009). This SLR may lead to significant land-surface inundation

* Corresponding author. Tel.: +98 912 2157662; fax: +98 21 66014828.
E-mail addresses: dmahmoodzadeh@alum.sharif.edu (D. Mahmoodzadeh), hketabchi@mehr.sharif.edu (H. Ketabchi), ataie@sharif.edu (B. Ataie-Ashtiani), craig.simmons@flinders.edu.au (C.T. Simmons).

http://dx.doi.org/10.1016/j.jhydrol.2014.07.010
0022-1694/

(LSI), particularly in low-topography small islands (Bricker, 2007; Ketabchi et al., 2014). Also, annual mean precipitation and therefore recharge rate could vary by up to ±50% (IPCC, 2013).

Ataie-Ashtiani et al. (2013b) briefly reviewed the recent studies regarding the SLR impact on unconfined shallow aquifers and they showed that LSI caused significantly more extensive SWI, with inland penetration up to an order of magnitude larger in some cases in unconfined coastal aquifers with realistic parameters, compared to the effects of pressure changes at the coastline. They also outlined some of the remaining research challenges in related areas, concluding that LSI impacts are among other important research questions regarding the SLR-SWI problems that have not been addressed, including the effects of real-world three dimensionality and the combined impacts of climate change. They also highlighted the lack of research on the SLR impacts for the groundwater resources of islands.

Masterson and Garabedian (2007) simulated a simplified hypothetical FGL similar to coastal aquifers found along the Atlantic coast of the United States considering the effects of SLR of 2.65 mm/year from 1929 to 2050 and recharge rate of 700 mm/year on the FGL shape using the SEAWAT model. Bailey et al. (2009) employed a conceptual model for atoll-island aquifers in a numerical modeling study to evaluate the response of the FGL to some controlling climatic and geologic variables. Payne (2010) considered the contribution of SLR (0, 0.3, and 0.6 m) and changes in precipitation patterns to the characteristics of SWI in the Hilton Head Island, South Carolina area using the SUTRA model. Rozell and Wong (2010) investigated SLR impacts on a small sandy island of Shelter located in New York State, United States, using SEAWAT. Predicted changes in recharge rate (540–640 mm/year) and SLR of 0–0.61 m over the next century were used to create three future climate scenarios. The model did not consider surface topography and the LSI that would occur under SLR. Sulzbacher et al. (2012) applied FEFLOW to estimate climate change impacts on the North Sea Island of Borkum. For simulating future changes in this coastal groundwater system, the climate change scenario until the year 2100 was specified based on climate change projections by IPCC (2007), combined with data for the German North Sea coast.

From an analysis and review of the literature, it can be concluded that no FGL studies have considered LSI impacts of SLR. Sefelnasr and Sherif (2014) investigated the possible effects of SLR in the Mediterranean Sea on the SWI problem in the Nile Delta Aquifer using FEFLOW considering the effect of the LSI, using digital elevation models. SLRs of 0.5 and 1 m in combination with 50% reduction and 200% increase in current groundwater pumping were considered. They showed that 19–32% of the total area of the Nile Delta became submerged due to the LSI.

Recently, Ketabchi et al. (2014) provided an extensive review on the influence of SLR on FGLs. They extended an explicit analytical steady-state, sharp-interface solution to study the behavior of FGLs influenced by SLR and LSI in two-layer oceanic islands. The impact of recharge rate, coastline slope, and geologic conceptualization (thickness and hydraulic conductivities) on the thickness and the volume of FGLs were studied. They clearly demonstrated that the inclusion of the two-layer geology leads to profound and significant changes to FGLs on small islands and that a one-layer model is overly simplistic in many cases. Their study concluded that FGL volumes and thicknesses were most sensitive to recharge rate, followed by coastline slope, aquifer layer thickness and hydraulic conductivity, rather than SLR impacts, in the range of parameters considered in their study. One of the main shortcomings of their work was considering simplistic hypothetical cases, without the real-world complexities, and this is also the case for other studies (Ataie-Ashtiani et al., 2013b). The real-world complexities such as three-dimensionality, irregularity in boundary shapes, aquifer layering contours, and topography are just a few matters that have not been considered. Understanding when and how these factors should be treated in both conceptual and numerical modeling remains an unresolved challenge and requires a systematic and quantitative evaluation in support of evidence based modeling decision making.

The objective of this work is to address the abovementioned shortcomings of previous work and to extend the work of Ketabchi et al. (2014) to a real-case study island in order to comprehensively investigate relationships between potential climate change scenarios and FGL responses. For this purpose, Kish Island, an arid-region case study, which has been extensively studied before (Ataie-Ashtiani et al., 2013a, 2014) is considered. The real case study allows a detailed exploration of processes that extend well beyond simplified and hypothetical analyses, whilst at the same time providing new insights about the Kish Island system as well as generalizable outcomes relevant to many island systems worldwide. Therefore, this work is novel because we provide a qualitative and systematic comparative study of the impacts of some important simplifications and conceptualization in the modeling processes, using the groundwater system of Kish Island rather than just providing a site-specific case or a completely hypothetical situation.

To provide a better understanding of the FGL dynamics, density-dependent groundwater modeling using SUTRA (Voss and Provost, 2010) is applied for this study which is a more accurate modeling approach in comparison with analytical solutions applied for example, by Ketabchi et al. (2014). Hence, the present paper describes the Kish Island modeling and highlights the potential limitations of such complex and real-case modeling, applied to quantify the influence of climate change factors on the FGL. Here, we address (1) how the conceptual aspects of real-case small island modeling (aquifer layering, lateral boundary geometries, unsaturated zone conditions, and dimensionality) affect the shape of the FGL, and (2) how the combined climatic parameters (including SLR, LSI, and variations in net recharge rate) potentially impact the FGL status. This is the first study to explore the range of potential conceptualizations and their impact on modeling results. The modeling results presented here can therefore help to guide better conceptual and numerical modeling for real island aquifer systems such as the one presented here.

2. Kish Island, Iran

Kish Island is located in the Persian Gulf, approximately 17 km off the southern coast of Iran at 26°29′ to 26°35′N latitude and 53°53′ to 54° 04′E longitude. It has a nearly elliptical shape with major axis in the west-east direction. In 2010, this island supported a population of about 84,200 including locals and tourists. Since the 1980s, this island has been a free trade zone and a highly well-known holiday destination. It is currently expected that about one million tourists visit this island once a year (Kish Free Zone Organization, 2006; Ataie-Ashtiani et al., 2014). Kish Island occupies a land area of about 90 km^2 and at its highest location rises to about 40 m above mean sea level (MSL). Fig. 1 shows Kish Island's location and its surface topography.

The geology of this island mainly consists of two layers. The upper layer contains condensed sand, coral sediments, lumachelle limestone, crushed coral and reef limestone shells discordantly overlying the formation of the thicker bedrock containing clay marl with lenses of silt that are denser and less permeable. Hydraulic conductivity measurements for the upper layer vary between 1.0×10^{-5} and 1.0×10^{-3} m/s while for base layer, they vary between 1.0×10^{-7} and 1.0×10^{-4} m/s (Ataie-Ashtiani, 2010; Ataie-Ashtiani et al., 2013a).

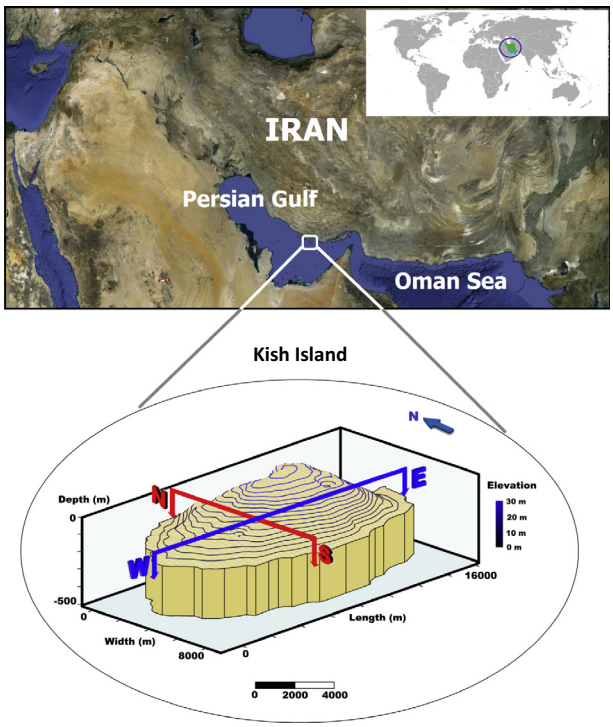

Fig. 1. Location map of the study area, Kish Island, Iran in the Persian Gulf.

In general, the area's climate is classified as an arid region (Ataie-Ashtiani et al., 2014). The mean annual rainfall of Kish Island is about 200 mm, with a high degree of annual variability (Kish Free Zone Organization, 2006). There is no significant runoff on this island. Accounting for groundwater extraction from the FGL for consumption purposes of irrigation or feeding desalination plants, the net recharge to the FGL is estimated to be about 10% of the mean annual rainfall (Preusser et al., 2003; Ataie-Ashtiani et al., 2013a, 2014).

In order to determine Kish Island's groundwater levels and salinities, field data from 62 previously drilled wells were used. Three sets of measurements were completed in November 2009, January 2010, and March 2010 as a part of Ataie-Ashtiani (2010) and Ataie-Ashtiani et al. (2013a) studies. Fig. 2 shows the locations of these wells and those considered in the present study for the calibration procedure. Much of the development on this island has occurred along the northern, eastern and north-eastern parts of the island. Therefore, as shown in Fig. 2, the wells are mostly drilled in close proximity to these areas. Based on the investigations of Ataie-Ashtiani et al. (2013a), (1) The groundwater flows radially toward the sea and the water table rarely exceeds 10 m above MSL, (2) The groundwater system is classified as a recharge-limited (flux-controlled) system and hence, unsaturated zone depths between 1.7 and 23.0 m on this island give rise to sufficient vadose zone thickness to influence the water table shape of FGL, and (3) The electrical conductivity measurements in abovementioned wells vary between 1026 μS/m and 55,600 μS/m.

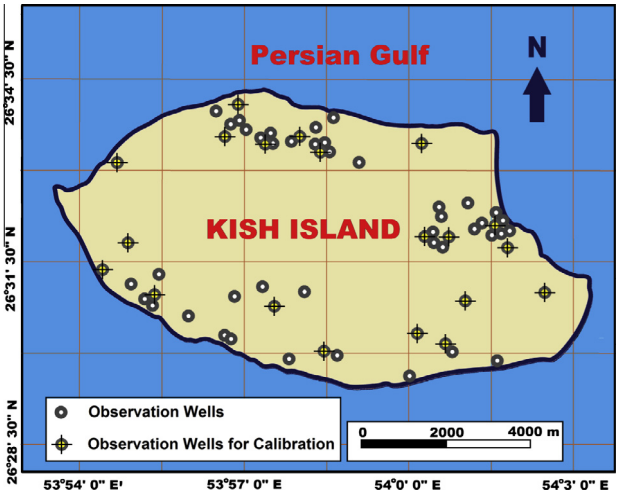

Fig. 2. The location of observation wells in Kish Island.

Further detailed information regarding geography, climate, hydrogeology, recharge estimates, water supply and other characteristics of this island are available in Ataie-Ashtiani (2010) and Ataie-Ashtiani et al. (2013a) and are not repeated here.

3. Numerical modeling

The FGL of Kish Island is simulated using both two-dimensional (2D) and three-dimensional (3D) numerical simulations using SUTRA (Voss and Provost, 2010). In the following, a brief description of the numerical modeling procedures is presented.

3.1. Spatial and temporal discretization

The 3D model of Kish Island is constructed in a manner similar to that employed by Ataie-Ashtiani et al. (2013a, 2014). The model domain is discretized to 18,000 hexahedral elements (20,808 nodes) with equal lengths of 500 m in the horizontal direction, and varying lengths of 2.19–27.11 m in the vertical direction. The appropriate depth in the vertical direction for simulation purposes is approximately 500 m below MSL. This depth ensures that the salinity distributions are not affected by domain size and is obtained after trial-and-error simulation testing with several depths in the range of 300–700 m.

The schematized N–S and W–E cross-sections used for 2D modeling with finite-element mesh, layering properties, and assigned boundary conditions are illustrated in Fig. 3a and b, respectively. The locations of these cross-sections are shown in Fig. 1. The non-uniform mesh for simulations is composed of 5849 and 8556 quadrilateral finite elements (6021 and 8777 nodes) for N–S and W–E cross-sections, respectively. In both cross-sections, the aquifer is divided into 50 layers of varying height of 1.23 m at the MSL to 33.86 m at the aquifer bottom in the vertical direction. The top elevation is spatially variable and corresponds with surface elevation, based on the compiled topography map of Kish Island. Above MSL, the model consists of constant 1 m thick elements, in the vertical direction. The mesh is refined near the top and near the sea boundaries of the domain where a steep change of hydraulic heads and salinities is expected. The horizontal size of the mesh for the N–S model with lateral distance of 7700 m, changes from 50 m in the zone near the sea to 100 m in central parts of the domain. Similarly, the mesh sizes ranged from 50 m to 275 m for W–E model, which has 14,000 m length. Following testing of various mesh sizes (up to two times coarser and finer than current choice), the abovementioned discretization for 3D and 2D models were adopted in accordance with the spatial stability criterion (the Peclet number is smaller than four) (Voss and Souza, 1987; Voss and Provost, 2010). The results of the mesh size analysis show an appropriate grid convergence and therefore, the solutions no longer change appreciably as a function of grid size.

The time step size is initially set equal to 1800 s and then successively increases by a multiplier factor of 1.2 within 10 time step cycles until it reaches a maximum allowed time step of 2.0×10^8 s for all models, respectively. Temporal discretization is based on

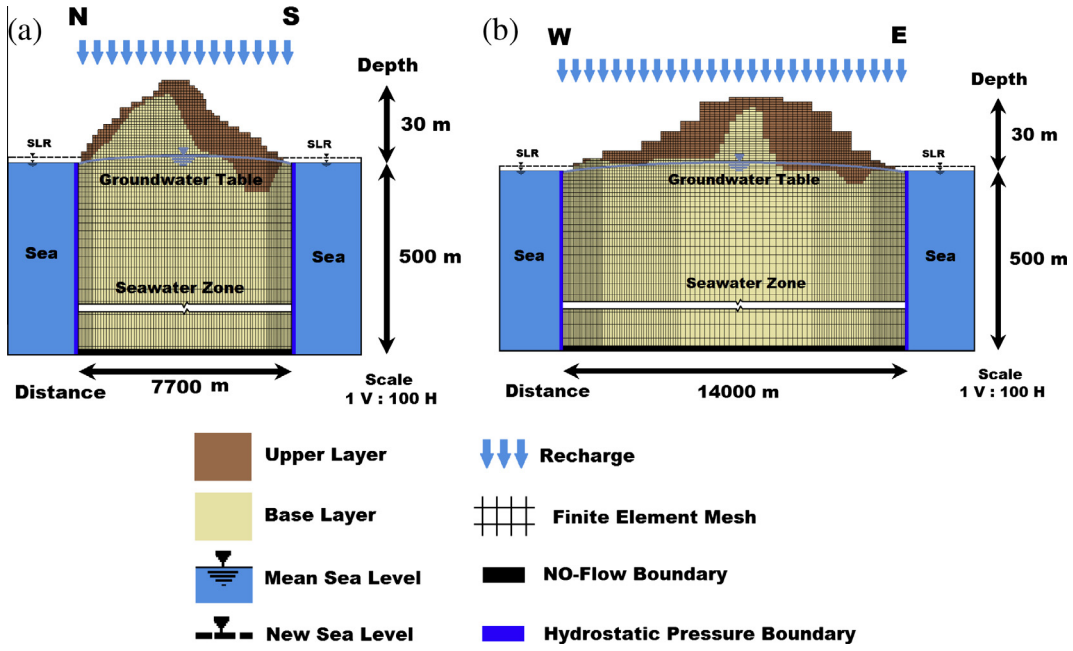

Fig. 3. (a) The N–S cross-section and (b) the W–E cross-section of Kish Island from Fig. 1.

stability criterion according to velocities and spatial discretization to ensure the courant number is smaller than 0.75, computational time, and required accuracy considerations (Voss and Souza, 1987).

3.2. Boundary and initial conditions

Specified pressure values are assigned to all of the nodes at sea boundary conditions and for those inundated by rising sea level. Freshwater sources are assigned to nodes on the surface of island where recharge enters the groundwater system. Solute boundary conditions consist of zero salinity for recharging the aquifer from the top and fixed salinity of 0.04 kg/kg [the salinity of the Persian Gulf (Nadim et al., 2008; Ataie-Ashtiani et al., 2013a)] on nodes at the sea boundaries. A no-flow boundary at the bottom surface (at a depth of 500 m below MSL) is assumed. The salinity gradient at the bottom surface is presumed to be zero. The boundary conditions applied in the present study are typical boundary conditions used in similar small island modeling studies e.g., Ghassemi et al. (2000), Ataie-Ashtiani et al. (2013a, 2014).

The 2D and 3D simulations start with seawater conditions everywhere beneath the land surface and continue to run for a time that is long enough to reach equilibrium. Steady-state equilibrium of the FGL is approached asymptotically and a cutoff is therefore assumed for the purposes of the analysis, after 8000 years. This final situation with FGL included is considered as an initial condition in the automatic calibration procedure.

3.3. Model calibration

The calibration procedure is based on the 3D model to provide the capacity to reliably use measured data in the available observation wells because of the spatial distribution of these wells. The calibration is carried out using the automated parameter estimation code PEST (Doherty, 2005) using the field measured salinity values in 20 available observation wells as shown in Fig. 2. As seen in Table 1, salinities in the considered wells were measured at different depths from MSL depending on the location of wells in Kish Island. These observation wells are chosen according to the reliability of measured data considering the existing historical information and also noting that the measured salinities in these wells are representative of spatial salinity distribution and free from local salinity fluctuations. The calibration procedure adopted by Ataie-Ashtiani et al. (2013a) is considered for this purpose. Similar to their procedure, the calibration and parameter estimations were carried out for the case of steady-state conditions for FGL. This is a commonly used assumption, particularly when reliable and sufficient records of transient and reliable data for a transient calibration are not available (Falkland, 1991; Ghassemi et al., 2000; Banerjee and Singh, 2011). However, a better approach is to consider uncertainty propagation analysis to account for unreliability or uncertainty in model structure and inputs (Rajabi and Ataie-Ashtiani, 2014). The recent advances in developing efficient uncertainty propagation analysis procedures pave further applications of this approach for real-world groundwater problems (Rajabi and Ataie-Ashtiani, 2014).

Following the procedure outlined by Ataie-Ashtiani et al. (2013a), the number of calibration parameters is limited to upper layer hydraulic conductivity and longitudinal dispersivity. The base layer hydraulic conductivity and transverse dispersivity are linked to upper layer hydraulic conductivity and longitudinal dispersivity with a factor of 0.1, respectively (Ataie-Ashtiani et al., 2013a). In Ataie-Ashtiani et al. (2013a), a wider and non-site-specific range of variations for calibration parameters (the range of 1.0×10^{-13} to 10.0 m/s for upper layer hydraulic conductivity and 5.0–500.0 m for longitudinal dispersivity) was adopted for the specific purpose of investigating feasible errors in the model structure. In this study, according to measured ranges for these parameters (Ataie-Ashtiani, 2010; Ataie-Ashtiani et al., 2013a), the range of calibration parameter targets is restricted to only those that are considered reasonable and realistic ranges of values for the site. In the present study, the range of 1.0×10^{-5} to 1.0×10^{-3} m/s is considered for the upper layer hydraulic conductivity and the calibrated value of 2.08×10^{-4} m/s is obtained. Table 1 presents the observation wells coordinates, measured and simulated salinities of the calibrated model.

Table 2 summarizes all the values of the input parameters, including the values of the calibrated parameters for the numerical models of this study. These parameters are the same as those adopted by Ataie-Ashtiani et al. (2013a, 2014) and also calibrated values. As seen in Table 2, the longitudinal and transverse

Table 1
Observation wells in calibration procedure with measured and simulated salinities.

Well number	Coordinate (m)			Measured salinity (kg/kg)	Simulated salinity (kg/kg)	Residual salinity (kg/kg)
	X	*Y*	*Z*			
1	10,165	3359	9.4	0.00135	0.00665	0.00530
2	10,724	3353	6.9	0.00134	0.00810	0.00676
3	7646	7042	−1.1	0.00285	0.01636	0.01352
4	6151	5809	0.8	0.00497	0.01208	0.00711
5	1902	4363	−1.3	0.00508	0.01731	0.01223
6	7038	1141	0.8	0.00248	0.01511	0.01263
7	5329	928	11.3	0.02773	0.01352	−0.01421
8	1403	2029	−3.6	0.03203	0.01868	−0.01335
9	13,528	4737	−1.1	0.00677	0.01924	0.01247
10	11,390	5233	−1.9	0.00272	0.01232	0.00961
11	10,145	6268	−1	0.00337	0.01225	0.00888
12	2769	5988	−1.9	0.01380	0.01505	0.00125
13	1254	5211	0	0.03140	0.03998	0.00858
14	4274	919	0.7	0.00180	0.01600	0.01420
15	10,966	6627	−1.9	0.00334	0.01489	0.01156
16	12,370	3571	−3.6	0.00375	0.01956	0.01581
17	12,048	2860	−1.8	0.00348	0.01424	0.01076
18	9726	581	−1.6	0.00934	0.01888	0.00954
19	4529	50	−11.3	0.00249	0.02337	0.02088
20	6306	832	−3.9	0.00215	0.01454	0.01239

Maximum error (kg/kg): 0.02088.
Minimum error (kg/kg): 0.00125.
Average error (kg/kg): 0.00830.
Absolute average error (kg/kg): 0.01105.

Table 2
Input parameters for the numerical models in this study.

Parameter	Value
Freshwater density (kg/m^3)	1000
Seawater density (kg/m^3)	1028
Freshwater concentration (kg/kg)	0
Seawater concentration (kg/kg)	0.04
Fluid dynamic viscosity (kg/m s)	0.001
Molecular diffusion (m^2/s)	1.48×10^{-9}
Fluid compressibility (m s^2/kg)	4.47×10^{-10}
Matrix compressibility (m s^2/kg)	1.0×10^{-8}
Gravitational acceleration (m/s^2)	9.81
Porosity	0.25
Net recharge rate (mm/year)	20
Upper layer hydraulic conductivity[a] (m/s)	2.08×10^{-4}
Base layer hydraulic conductivity[a] (m/s)	2.08×10^{-5}
Longitudinal dispersivity[a] (m)	103.1
Transverse dispersivity[a] (m)	10.3
Residual saturation	0.3
Van Genuchten (1980) curve fitting parameter (1/m)	0.5
Van Genuchten (1980) pore size distribution index	2

[a] Based on calibration procedure.

dispersivity values of 103.1 m and 10.3 m, respectively (obtained by the calibration procedure) are on the order of dispersivity values used in studies with similar spatial scales (e.g., Gelhar et al., 1992; Xu and Eckstein, 1995; Yakirevich et al., 1998; Mehta et al. 2000; Shamrukh et al., 2001; Werner and Gallagher, 2006). The unsaturated zone in this island is also simulated in SUTRA using Van Genuchten formulations (Van Genuchten, 1980).

The initial condition of all simulations scenarios is based on the long-term quasi-steady-state simulation. In each numerical simulation scenario, the total simulation time is set to be on the order of thousands of years to reach a new steady-state with the purpose of the prediction of long-term impacts under the considered scenarios (e.g., SLR and recharge rate variations).

4. Conceptual model

The general conceptual model of Kish Island is developed based on the data collected and analyzed from physical parameters and hydrogeological properties of the island aquifer (Ataie-Ashtiani, 2010; Ataie-Ashtiani et al., 2013a, 2014). While the conceptual model is an idealized summary of the current understanding of the FGL condition and the key aspects of how the flow system works, it is subject to some simplifying assumptions. Most importantly, the assumptions are required partly because a complete reconstruction of the field system is not feasible largely because there is insufficient data for a complete description of the system (Falkland, 1991; Underwood et al., 1992; Middlemis, 2000). In this section, we outline some specific and important features that we hypothesize may have little or large impacts on the model results when model simplification and conceptualization is undertaken. The overall objective of developing the appropriate conceptual model is to test the influence of the aquifer layering and geometry, and also, understand how the unsaturated zone conceptualization affects the simulation results. All of the investigations to understand model conceptualization choices are performed using 2D steady-state simulations of Kish Island's N–S and W–E cross-sections under the proposed conceptual framework.

4.1. Aquifer layering impact

Ketabchi et al. (2014) showed that layering properties in small islands are essential aspects in FGL shapes and volumes. Coral, volcanic, limestone, sandy and atoll islands are examples of small islands consisting of two-layer aquifer systems. A list of these types of islands was summarized in their study. Kish Island consists of two distinct hydrogeological layers. The hydraulic conductivity of the upper layer is greater than that of the base layer. This is very typical of such small sandy islands (e.g., Rozell and Wong, 2010; Praveena et al., 2011; Ketabchi et al., 2014). Two different cases are considered here. For the first case, the aquifer is considered to be a single-layer and in the second case the two-layer aquifer is considered. In the single-layer aquifer, the upper layer properties are neglected and the entire domain is considered to be made of base layer only. Fig. 4a and b shows the salinity profiles (only the 10%, 50%, and 90% salinity contours from the transition zone are illustrated) in the N–S and W–E cross-sections for these two cases, respectively.

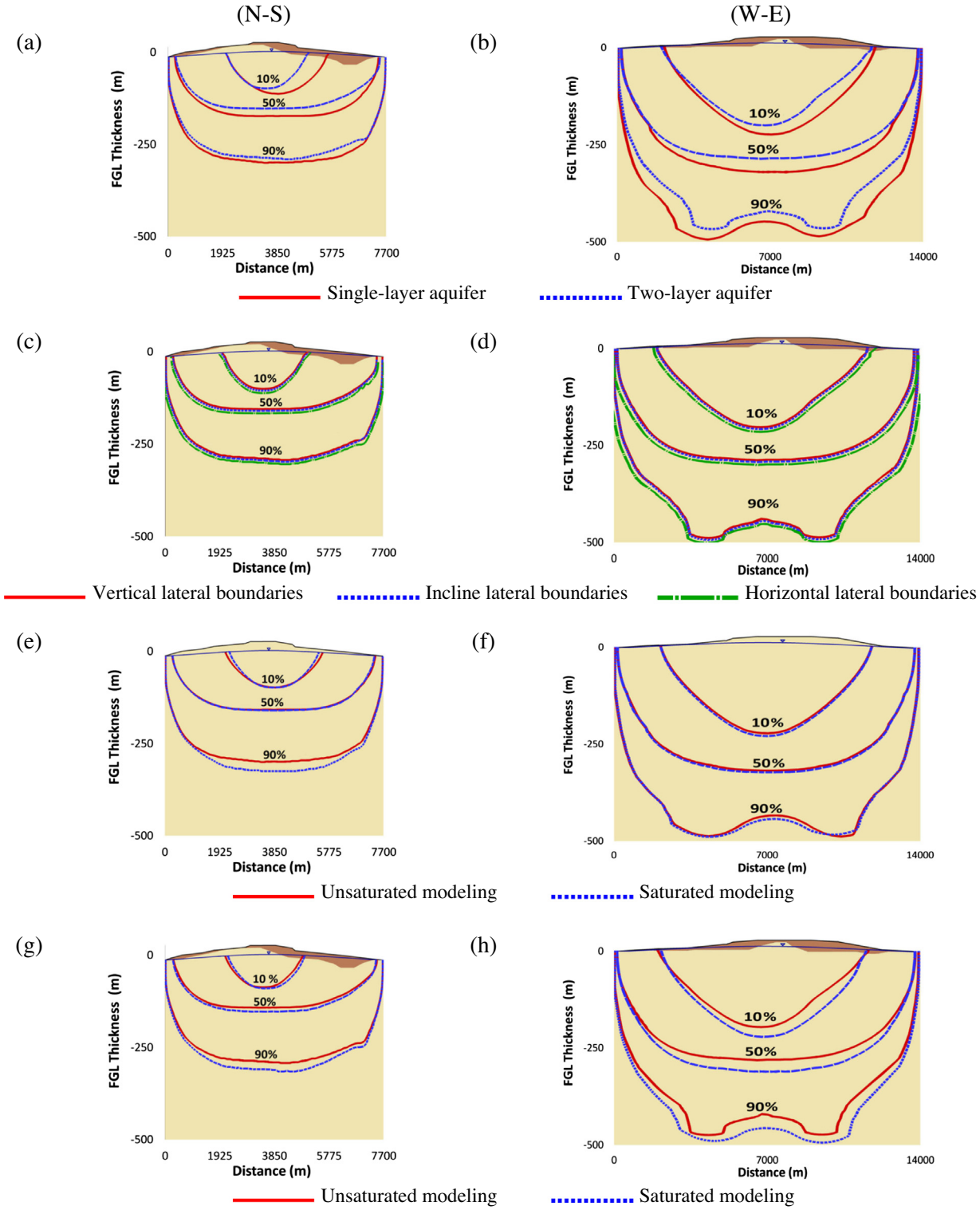

Fig. 4. The salinity profiles, (a-b) single-layer and two-layer systems, (c-d) vertical, incline, and horizontal lateral boundaries, (e-f) unsaturated and saturated groundwater flow modeling in single-layer system, (g-h) unsaturated and saturated groundwater flow modeling in two-layer system, for the N–S and W–E cross-sections.

In order to provide an additional evaluation between the results obtained from the numerical simulations of the present study and the analytical solution introduced by Ketabchi et al. (2014), the maximum FGL thicknesses in the N–S and W–E cross-sections can be compared. The maximum FGL thickness is considered as the point of intersection of the 50% salinity contours. It can be seen from Fig. 4a that the maximum FGL thicknesses are 140.6 m and 172.0 m for N–S cross-section under single-layer and two-layer conditions using the numerical simulations, respectively. Smaller thicknesses of 111.1 m and 127.8 m are estimated using the analytical solution of Ketabchi et al. (2014) for similar conditions. Furthermore, on the basis of the abovementioned analytical solution, the maximum FGL thicknesses at the W–E cross-section of island are 204.7 and 232.3 m for single-layer and two-layer conditions, respectively. However, the numerical simulation results indicate a thicker FGL, equal to 282.0 and 321.1 m for the same cases (Fig. 4b). As described

by Ketabchi et al. (2014), the analytical solutions are based on a number of simplifications, such as sharp interface, hydrostatic equilibrium of seawater and freshwater, the lack of a discharge zone at the coastline and horizontal flow of freshwater. Therefore, the results are not exactly the same for the analytical solution and numerical simulations. The comparison provides confidence in the results of the approach employed in the present study.

It can be concluded that the FGL simulation of the two-layer aquifer, in the case of Kish Island, indicates a smaller thickness of the FGL and it is in agreement with the results of Ketabchi et al. (2014). In this condition, the FGL position is highly controlled by the geologic layering and the value of hydraulic conductivity and thickness of each layer. The greater hydraulic conductivity of the upper layer in comparison to that of the base layer in small sandy islands such as Kish Island studied here shows that the FGL is limited in thickness by the ratio of the layer's hydraulic conductivity values. This behavior often contrasts to atoll island characteristics (Schneider and Kruse, 2006; Rozell and Wong, 2010; White and Falkland, 2010; Ketabchi et al., 2014). The results clearly demonstrate that the assumption of the two-layer geology leads to profound changes in the FGL and highlights the importance of the layering conceptualization on the Kish Island FGL prediction and analysis. Therefore a one layer conceptualization cannot be applied as it would lead to significant errors in FGL prediction.

4.2. Aquifer geometry impact

The FGL modeling for real cases of small islands that include complex island geometries and its stratigraphy have been included in the various models available in the literature (e.g., Schneider and Kruse, 2006; Kopsiaftis et al., 2009; Oude Essink et al., 2010; Rozell and Wong, 2010; Payne, 2010; Praveena et al., 2011; Sulzbacher et al., 2012; Sefelnasr and Sherif, 2014). Complex geometry patterns can be comprised of the topography of the study domain, irregularity of coastlines, variable thickness of formations, variations in formation depth, and the location and geometry of the lateral aquifer boundaries (Falkland, 1991; Abarca et al., 2007). Here, a numerical methodology is employed to evaluate the impact of the lateral aquifer boundary geometry on the FGL simulation. The topography, coastlines, and layering properties of Kish Island are based on available data. Kish Island consists of irregular lateral boundaries (Drees and Sommer, 2004; Ataie-Ashtiani, 2010). The impact of the form of the lateral boundaries on the FGL position is studied using simulations that include the lateral slope of the island. For this purpose, the N–S and W–E cross-sections of Kish Island in the cases of vertical, incline, and horizontal lateral boundaries are considered. A schematic of N–S and W–E cross-sections of such aquifers are presented in Fig. 5. For incline boundaries, we assume a 1:1 lateral slope while for the cases of horizontal boundaries, the model domain extends an additional 3000 m offshore at both sides.

In order to compare the result of the simulations, the salinity profiles for the cases of all vertical, incline, and horizontal lateral boundaries are shown in Fig. 4c and d. As seen, the FGL position is not significantly affected by the inclined boundary. This result, for the case of FGLs or deep coastal aquifers, is in agreement with findings of Abarca et al. (2007) for shallow coastal aquifers. When the slope of the aquifer is considered, the FGL is slightly (less than 1%) greater than in the case where it is not. Consequently, for most practical applications, the irregularities of coastal slopes including the bathymetry of sea bottom can be neglected without any significant influence of the results of the FGL numerical simulation.

4.3. Saturated or unsaturated groundwater flow modeling

The unsaturated zone is typically only a few meters thick in small islands and its influence on FGL shape and position is usually neglected in most of small islands (Falkland, 1991; Underwood et al., 1992; Stoeckl and Houben, 2012). In this section, we consider two conceptualizations to investigate the effects of an unsaturated zone on FGL position of Kish Island. The cases considered for the Kish FGL modeling are: (1) inclusion of unsaturated zone modeling (e.g., Sulzbacher et al., 2012; Sefelnasr and Sherif, 2014; Ketabchi et al., 2014), and (2) fully-saturated groundwater flow modeling with the unsaturated zone removed from the modeling domain (e.g., Voss and Souza, 1987; Underwood et al., 1992; Ghassemi et al., 2000; Rozell and Wong, 2010). Both conceptualizations of the unsaturated zone effect are schematized in Fig. 6. The present study is, to the authors' best knowledge, the first to systematically and quantitatively compare these two conceptualizations regarding the effects of unsaturated zone on FGL features. For our steady-state cases, we use the same recharge rate values in both conceptualizations of unsaturated zone, as our goal in this section is to investigate the influence of unsaturated zone implementation in the numerical model as seen in Fig. 6. The assumption of the same recharge rates use was confirmed by Flint et al. (2000) and Hunt et al. (2008). Flint et al. (2000) mentioned that travel time through the unsaturated zone is controlled by net infiltration, unsaturated zone thickness, and effective porosity. They also showed that under steady-state conditions, net infiltration becomes recharge, except when perched water is discharged in springs and lost to evapotranspiration. Hunt et al. (2008) demonstrated that consideration of flow through the unsaturated zone and recharge rate to groundwater system may be important when simulating the transient behavior of an aquifer. In thicker unsaturated zones, the long-term average volume of infiltrated water was properly simulated when using a fully-saturated groundwater flow modeling approach, but the timing and short-term rate of recharge were incorrect (Hunt et al., 2008).

Both cases are implemented for the N–S and W–E cross-sections that consider both single-layer and two-layer aquifer systems. The position of the FGL for both conceptualizations including an unsaturated zone is shown in Fig. 4e–h. For the single layer, the inclusion of an unsaturated zone gives approximately the same FGL as the fully saturated conceptualization. However for the two-layer case, the differences are far more significant. The differences in the FGL position of two-layer aquifer systems is related to layering properties of the porous media in the saturated and unsaturated zone such as the upper-layer thickness and hydraulic conductivity. Obviously, the first conceptualization that considers the influence of unsaturated zone is more realistic. Therefore in two-layer aquifers such as Kish Island, the inclusion of an unsaturated zone is both the more accurate and preferred approach for FGL modeling. This result also suggests that, instead of unsaturated groundwater flow modeling, one can simply remove the unsaturated zone if the aquifer system is single-layer, the thickness of the unsaturated zone is small, and the objective of the study is not to understand the detailed dynamics within the unsaturated zone or the interactions between the saturated and unsaturated zones. This approximation is particularly applicable to large-scale 3D systems when unsaturated flow modeling becomes computationally intensive because finer discretization is necessary (Voss and Provost, 2010).

Furthermore, the water table for the N–S and W–E cross-sections considering both the single-layer and two-layer aquifer system is illustrated in Fig. 7 with unsaturated zone effects. When an unsaturated modeling approach is employed, the water table can easily be estimated. The location of the water table corresponds to the zero-pressure values in the domain. Alternatively, the water table estimated using the saturated modeling approach can be estimated by converting the pressure values at the top boundary to corresponding head values. These procedures are used for water table location estimation of the N–S and W–E cross-sections. Comparable results from both conceptualizations are

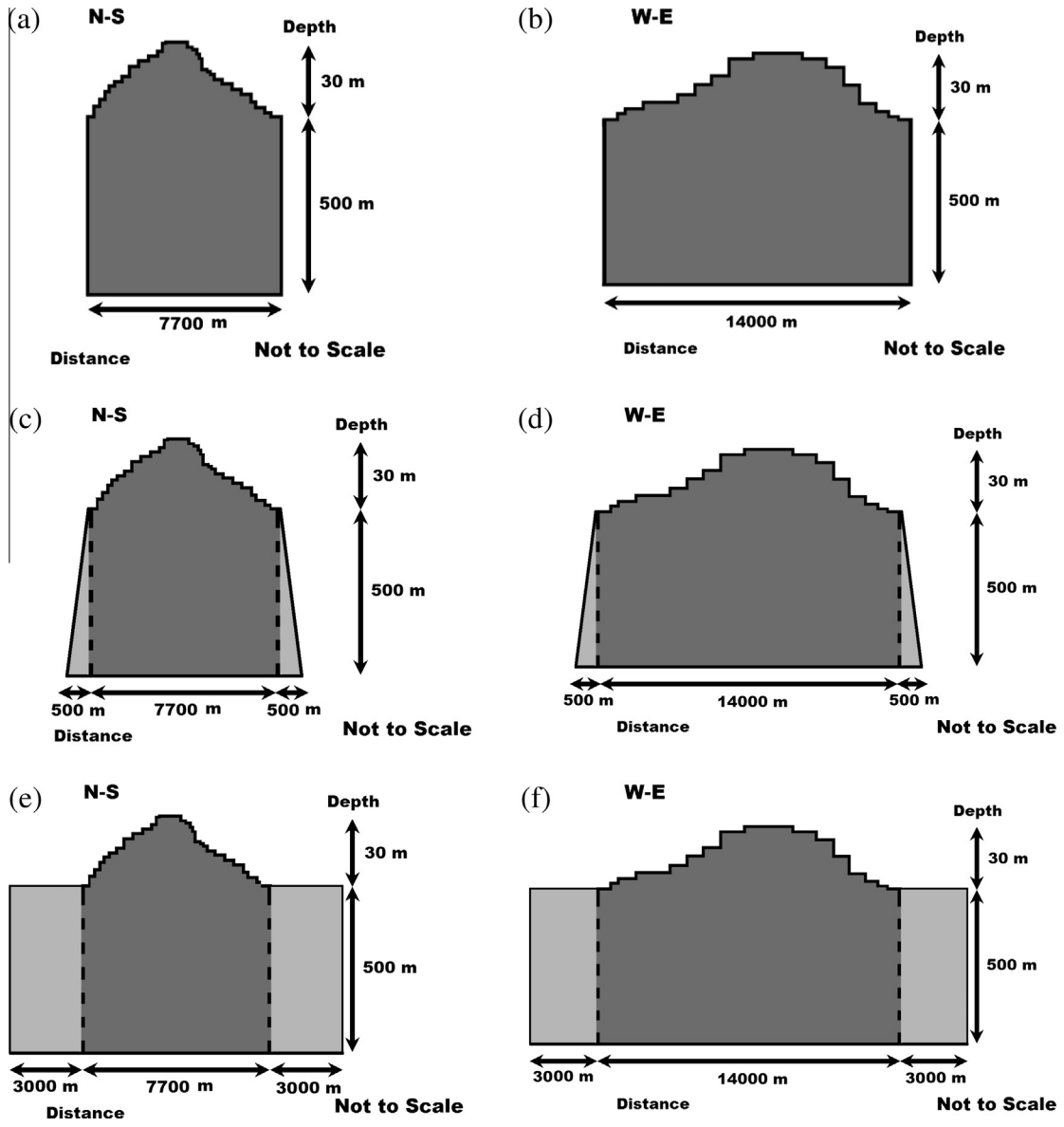

Fig. 5. Schematic of (a-b) vertical lateral boundaries, (c-d) incline lateral boundaries, (e-f) horizontal lateral boundaries, for the N–S and W–E cross-sections.

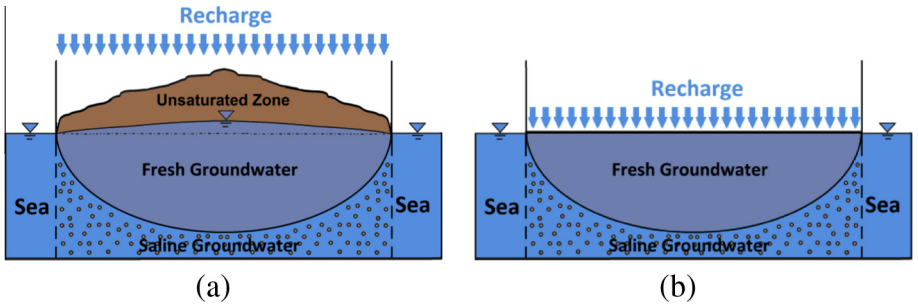

Fig. 6. Conceptual model of the FGL system in (a) unsaturated groundwater flow modeling (b) saturated groundwater flow modeling.

obtained as shown in Fig. 7a–d for a single-layer aquifer system while for a two-layer aquifer system, different water tables are predicted, as expected.

Understanding these conceptualizations is also important for accurate investigation of climate change impacts. Using the unsaturated modeling concept, recharge-limited or flux-controlled systems can be simulated accurately. Where such systems exist (e.g., in arid regions), less vulnerability to SLR is observed, because the hydraulic gradient between the land and sea can be maintained. However, in fully-saturated aquifers, such as those that are topography-limited or in head-controlled systems in low-topography regions, more vulnerability to SLR is expected. This is because the hydraulic head on the freshwater boundary cannot adjust in response to the seaward boundary changes

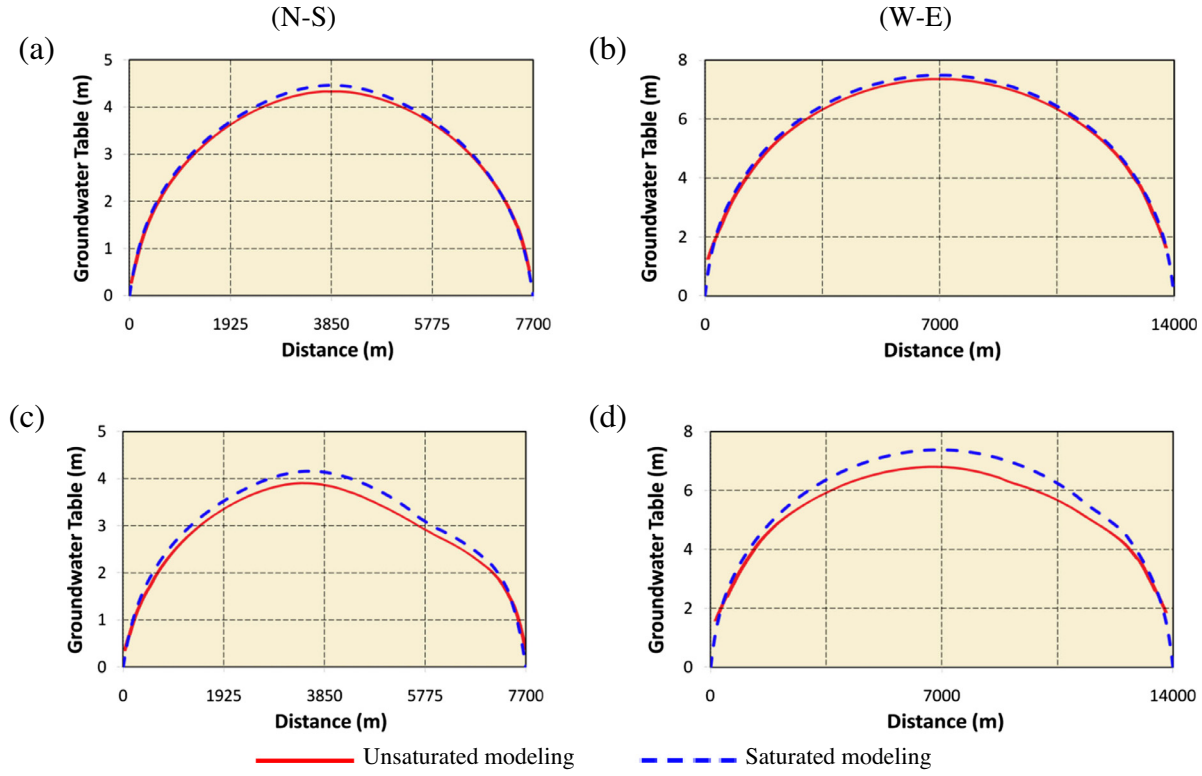

Fig. 7. Water table in unsaturated and saturated groundwater flow modeling (a) single-layer aquifer system for the N–S cross-section, (b) single-layer aquifer system for the W–E cross-section, (c) two-layer aquifer system for the N–S cross-section, (d) two-layer aquifer system for the W–E cross-section.

(Ataie-Ashtiani et al., 1999, 2001; Werner and Simmons, 2009; Michael et al., 2013).

In the following section, the climate change scenarios are studied for the Kish Island FGL using numerical simulations, based on the conceptualization explored in this section. Therefore, the two-layer aquifer of Kish Island is considered in which the lateral slope of aquifer is neglected. Also, unsaturated groundwater flow modeling is implemented in the simulation procedures.

5. Climate change scenarios

The most direct influences of climate change on groundwater resources of small islands are caused due to SLR and changes in recharge rate (e.g., Ketabchi et al. 2014). The conceptual model developed in this study allows the effects of various climatic factors to be analyzed. Table 3 summarizes these climate change scenarios. Four sets of the coupled realistic scenarios mimicking climate change are considered and denoted by ANLS, ALS, WLS, and DLS cases, as introduced in Table 3. Instantaneous SLR (a worst-case), similar to the approach applied by e.g., Watson et al. (2010), Chang et al. (2011), Michael et al. (2013), Sefelnasr and Sherif (2014), and Ketabchi et al. (2014) is considered. SLR scenarios of (1) NO-SLR condition, (2) SLR of 1 m based on IPCC (2013) prediction, and (3) SLR of 4 m, double the maximum rising predicted by Vermeer and Rahmstorf (2009) are explored (e.g., Chang et al., 2011). In the first set of scenarios, the coastline is maintained at its present location and the effect of the submergence of low-topography lands, LSI, by seawater as a result of SLR is not considered. In the three other remaining sets of scenarios the impact of LSI is considered. Furthermore, based on the recharge rate predictions (IPCC, 2013; Bricker, 2007; Sulzbacher et al., 2012), three net recharge scenarios are considered: (1) average scenario i.e., the current annual recharge rate of 20 mm/year, (2) wet scenario considering increasing the annual recharge rate of 20% (24 mm/year), and (3) 15% decreasing annual recharge rate for the dry scenario (17 mm/year).

Table 3
Climate change scenarios included in the numerical simulations.

Scenario	SLR (m)	LSI	Net recharge	
			Change (%)	Rate (mm/year)
ANLS0	0	No	0	20
ANLS1	1	No	0	20
ANLS4	4	No	0	20
ALS0	0	Yes	0	20
ALS1	1	Yes	0	20
ALS4	4	Yes	0	20
WLS0	0	Yes	+20	24
WLS1	1	Yes	+20	24
WLS4	4	Yes	+20	24
DLS0	0	Yes	−15	17
DLS1	1	Yes	−15	17
DLS4	4	Yes	−15	17

ANLS: Average recharge rate with No-LSI consideration for SLR.
ALS: Average recharge rate with LSI consideration for SLR.
WLS: Wet recharge rate with LSI consideration for SLR.
DLS: Dry recharge rate with LSI consideration for SLR.

6. Results and discussion

6.1. Steady-state FGL positions based on 2D results

The steady-state salinity distributions for the N–S and W–E cross-sections for the considered scenarios are plotted in Fig. 8a–h, respectively. The system is simulated for a long time (about 8000 years) to reach a new steady-state condition after imposing the impacts of climatic change. Note also that the long-term results

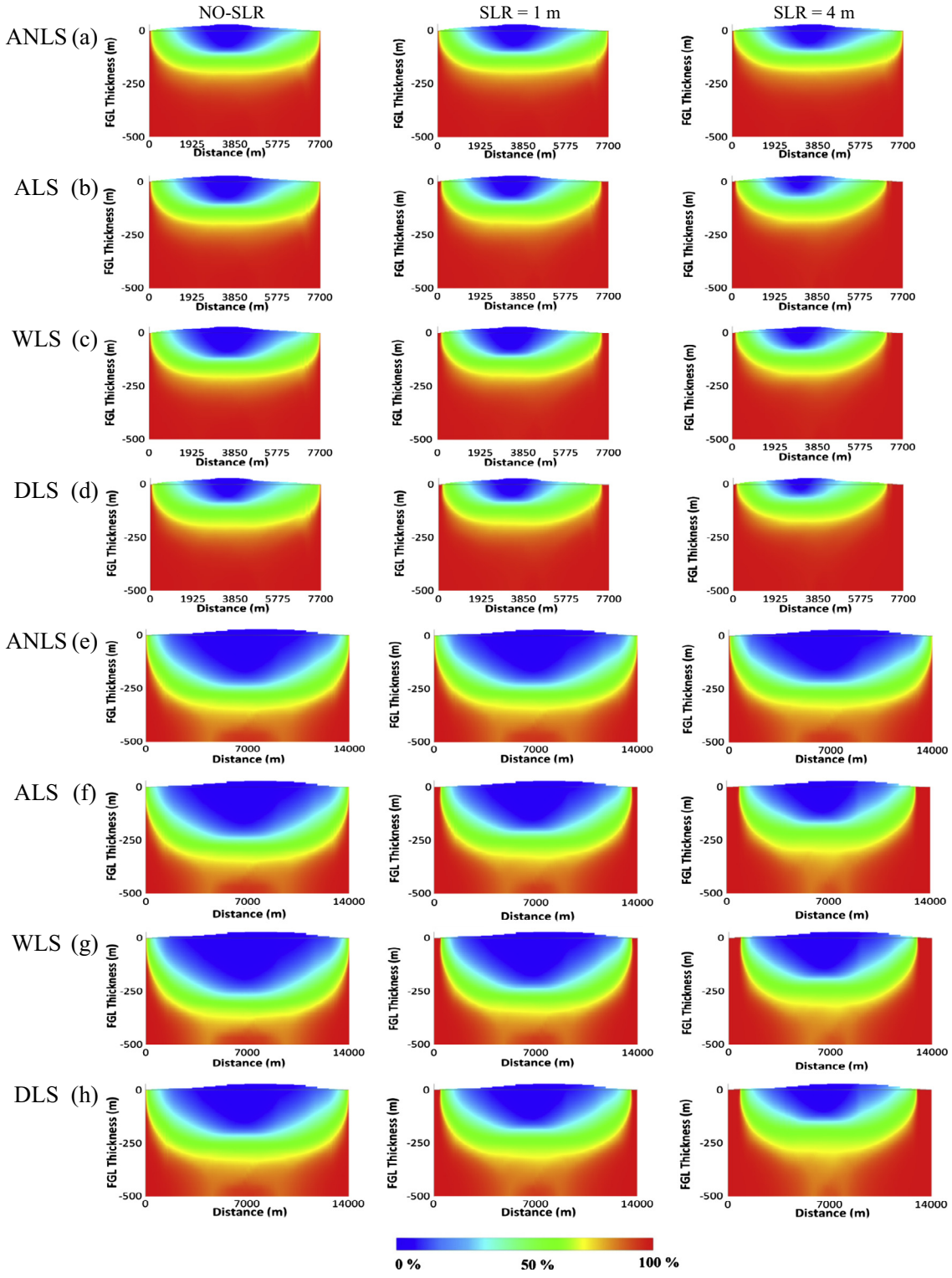

Fig. 8. Steady-state salinity distributions in the considered scenarios: (a-d) for the N–S cross-section and (e-h) for the W–E cross-section.

are an indicator of the potential impact and are a worst-case estimation of climate change impacts. Such analyses are similar to approaches adopted in the previous studies e.g., Chang et al. (2011), Webb and Howard (2011), Michael et al. (2013). The purpose of the average recharge rate and NO-SLR steady-state simulation (ALS0 scenario) is to estimate the FGL position that would exist in the system without considering the SLR and changes in recharge rate (base-case scenario).

The maximum FGL thicknesses, determined from MSL (considered as the point of intersection of the 50% salinity contours) and the percentage of changes in comparison to the base-case scenario are summarized in Table 4. The ANLS and ALS scenarios are the cases that the recharge rate variations are not considered in order to determine the behavior of the FGL only due to SLR. SLR impacts can be examined with LSI or without LSI effects and this issue is one of the main focuses of these two scenario assessments. When

Table 4
The maximum FGL thicknesses for the considered climate change scenarios.

Scenario	N–S cross-section		W–E cross-section	
	Thickness (m)	Change (%)	Thickness (m)	Change (%)
ANLS0	140.6	–	282.0	–
ANLS1	137.7	−2.1	277.0	−1.7
ANLS4	128.7	−8.4	267.3	−5.2
ALS0	140.6	–	282.0	–
ALS1	126.2	−10.2	256.0	−9.2
ALS4	111.6	−20.6	214.7	−23.8
WLS0	153.3	+9.1	309.8	+9.9
WLS1	138.7	−1.3	281.0	−0.3
WLS4	123.1	−12.4	237.1	−15.9
DLS0	131.6	−6.3	259.9	−7.8
DLS1	116.2	−17.4	236.2	−16.2
DLS4	101.9	−27.5	196.3	−30.4

LSI effects are not considered, a landward shift of coastline due to SLR is ignored as a simplifying assumption in the model. For given values of SLR, minor changes on the FGL shape and thickness are observed when the LSI impact is not considered, as shown in Fig. 8 for ANLS scenarios. These reduced impacts of SLR are due to the recharge-limited conditions of Kish Island as also observed in previous works e.g., Werner and Simmons (2009), Ataie-Ashtiani et al. (2013b), and Michael et al. (2013). ALS scenario results show that LSI intensifies the impact of SLR on the FGL, as indicated in Table 4. As seen, for instance, the maximum FGL thickness is decreased 10.2% and 20.6% corresponding to SLR of 1 and 4 m for N–S cross-section with LSI consideration whereas the proposed thickness only decreased by 2.1% and 8.4% for similar SLRs without LSI consideration in comparison with the base-case scenario. Therefore, it is seen that LSI has a considerable impact in comparison to cases where only the vertical effect of SLR is considered. This finding for Kish Island is in agreement with the results of Sefelnasr and Sherif (2014) for shallow aquifers and Ketabchi et al. (2014) results for island FGLs. Also, as Rozell and Wong (2010) noted, low-lying areas that are likely to be inundated or intersect with the SLR will experience more freshwater loss. Using this concept, near-sea lands with elevations below the elevation of sea (after SLR) are inundated by seawater (modeled as a hydrostatic pressure above seawater in ALS cases). The length of the FGL is generally constant under ANLS scenarios while it is reduced in ALS cases as illustrated in Fig. 8. This behavior is due to inundation of low-topography and near-sea lands of the island by SLR. Also, the transition zone which separates freshwater from seawater at the FGL boundary, thickens slightly in the all positions by SLR. A larger SLR creates a flatter FGL shape, which is also thinner (Falkland, 1991; Sulzbacher et al., 2012; Ketabchi et al., 2014).

Here, WLS and DLS scenario sets represent the propensity for SWI to occur in response to sustained and long-term changes in net recharge on the FGL. The cases of WLS0 and DLS0 investigate the impact of only recharge rate change under +20% and −15% variations in comparison to the average condition (20 mm/year) in the absence of any SLR. The steady-state maximum changes in FGL thicknesses are −6.3 to +9.1% (N–S cross-section) and −7.8 to +9.9% (W–E cross-section) (see Table 4) relative to the base-case scenario, respectively. Therefore, a change in recharge rate has a large impact on the FGL under the recharge-limited conditions of this Island. This agrees with the previous results of Ghassemi et al. (2000), Schneider and Kruse (2006), Praveena et al. (2011), and Ketabchi et al. (2014).

The FGL shape when subject to coupled SLR and recharge rate impacts for steady-state condition are investigated using WLS1, WLS4, DLS1, and DLS4 scenarios. All WLS and DLS scenarios have the influence of both SLR and recharge rate changes. As expected, the dryer DLS scenarios, with a 15% reduction in the recharge rate, lead to a thinner FGL than the wetter WLS scenarios with a 20% increase in recharge rate. Generally, the FGL shape is qualitatively similar to the cases where SLR and recharge rate changes are considered separately. These analyses indicate that changes in recharge rate have the potential to both mitigate and magnify the SWI impacts caused by SLR.

Table 4 provides the maximum thickness of FGL and their relative variations in comparison to the base-case scenario for various climate change scenarios. The percentages of the variations for WLS0, WLS1, and WLS4 scenarios are +9.1%, −1.3%, and −12.4% at the N–S cross-section and +9.9%, −0.3%, and −15.9% at the W–E cross-section. Therefore, the increase of the recharge (WLS0) thickens the FGL. However, SLR including LSI impacts thins out the FGL and when both impacts, of SLR and recharge increase, are considered together (WLS1 and WLS4) the FLG thickness reduces in these scenarios.

As seen in Fig. 8, the smallest FGLs are established when both recharge reduction and SLR with LSI (DLS1 and DLS4) occurred in the considered scenarios. The FGL thickness variations are −6.3%, −17.4%, and −27.5% at the N–S cross-section and −7.8%, −16.2%, and −30.4% at the W–E cross-section for DLS0, DLS1, and DLS4 scenarios, respectively (Table 4). Thus, it also confirms cumulative impacts of SLR and recharge rate reduction and a lower recharge rate intensifies the impacts of SLR.

6.2. Transient FGL positions based on 2D results

The transient variations in the maximum FGL thickness predicted for the N–S and W–E cross-sections are compared in Fig. 9 for the considered scenarios (Fig. 9a and b: ANLS scenarios, Fig. 9c and d: ALS scenarios, Fig. 9e and f: WLS scenarios, Fig. 9g and h: DLS scenarios). The similar behavior is observed in the following transient simulations with the three different ANLS, ALS, and DLS scenarios and shows the expected thinning of the FGL as sea level rises and recharge rate decreases. The cumulative and inverse impacts of DLS and WLS scenarios are also observed in the transient behavior of the FGL. Transient simulations highlighted that the climate change impacts on the FGL are slow and a new long-term steady-state condition is reached after several hundred years with Kish Island's hydrogeological properties (e.g., due to small hydraulic conductivity of each geological layer). It is seen in Fig. 9 that the FGL response to recharge rate is slightly faster than SLR. Therefore, the time to equilibrium may be significantly longer for the SLR scenarios. Because the climate change impact on the FGL is generally a slow process, it is likely that the proposed effects will lead to changes in the FGL conditions that will extend for centuries or longer, as confirmed by the results of this study, even if climate change itself (as a forcing function on the aquifer) is mitigated within coming decades.

6.3. Steady-state FGL positions based on 3D results

Steady-state salinity distributions under average recharge rate and NO-SLR condition (base-case scenario), using the 3D model are presented in Fig. 10. Also, the comparisons of the steady-state FGL for scenarios of ALS0, WLS0, DLS0, ALS1, WLS1, and DLS1 using the 3D model are shown in Fig. 11. The results of the 3D simulation of the FGL influenced by climatic factors are similar to the 2D simulations results in general, although some differences between the values of salinities can be observed. The predicted SLR could significantly alter the position of the island coastline and inundate near sea low-lying lands, especially in eastern north parts of island. The locations of N–S and W–E cross-sections are shown in Fig. 11.

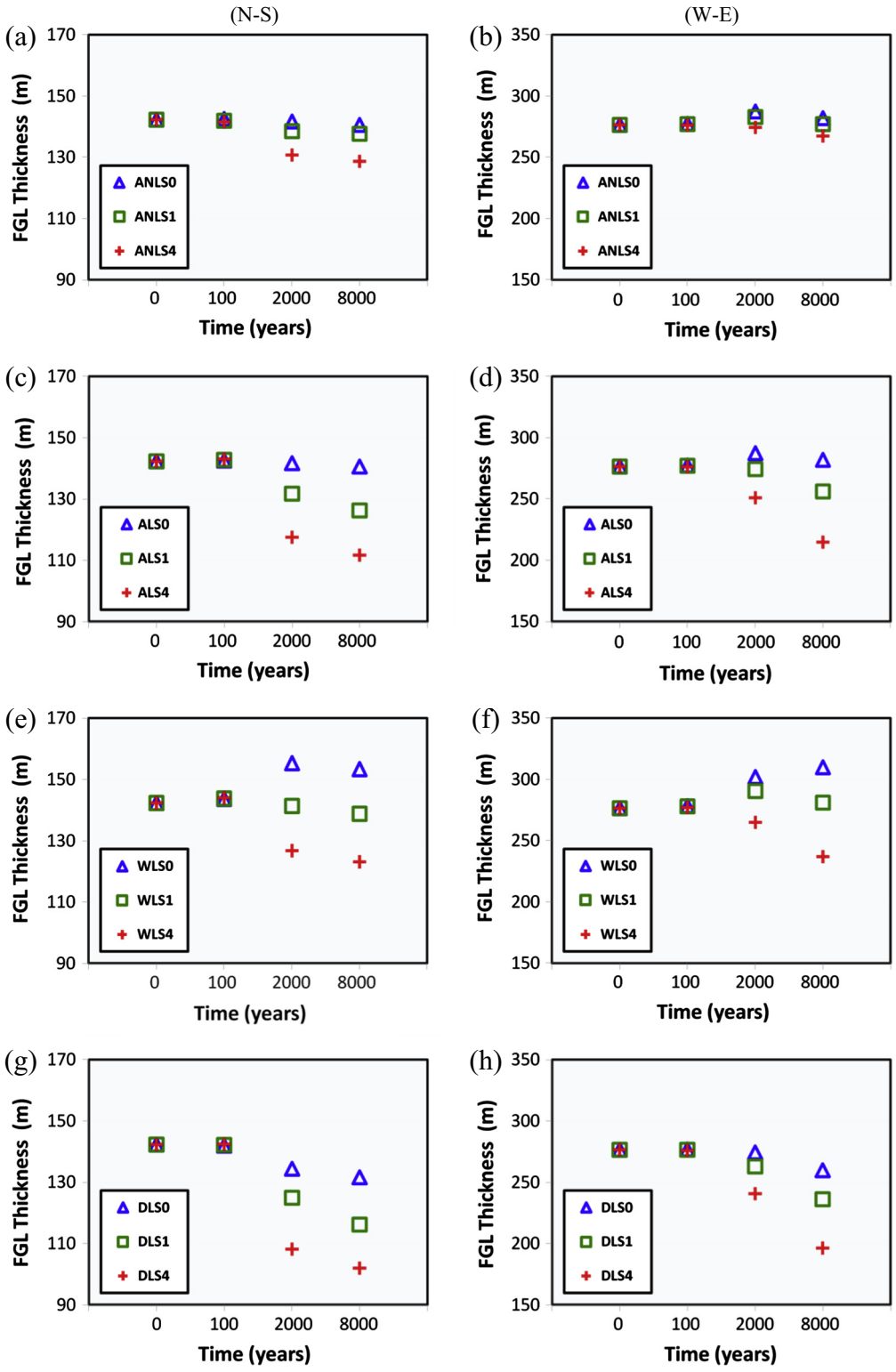

Fig. 9. Comparison of transient variations in the maximum FGL thickness predicted (a-b) for the ANLS considered scenarios, (c-d) for the ALS scenarios, (e-f) for the WLS scenarios, and (g-h) for the DLS scenarios, for the N–S and W–E cross-sections.

6.4. Evaluation of dimensionality impact

The maximum FGL thicknesses at the locations of N–S and W–E cross-sections are given in Table 5, for ALS, WLS, and DLS scenarios. As seen for N–S cross-section, regardless of the consistency between 2D and 3D results, the FGL thickness obtained using the 3D model for ALS0, WLS0, and DLS0 scenarios in which only the recharge rate changes were considered, are less than those of the corresponding 2D model. However, for ALS1, WLS1, and DLS1 scenarios in which coupled impacts of both SLR and recharge are implemented, the thickness of the FGL estimated by the 3D model is greater than those obtained by the 2D model. However, for the location of the W–E cross-section, the significant difference between the FGL thicknesses is visible and the FGL, simulated in

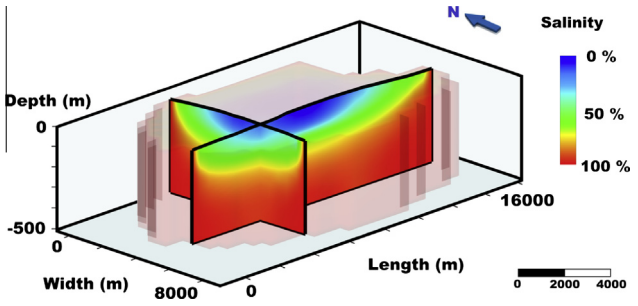

Fig. 10. Steady-state salinity distributions for base-case scenario using 3D modeling.

the 3D model, is thinner than 2D one. For instance, the maximum FGL thickness of 133.3 m is estimated by the 3D model for ALS1 scenario, while the maximum FGL thickness of 256.0 m is obtained for similar condition using the 2D model. This considerable difference, for the W–E cross-section is likely to occur because of the smaller width of the island in the north–south direction, not captured by 2D modeling. It is apparent from Table 5 that the average difference of 48.2% (134.1 m) in the FGL thickness is demonstrable while this average difference at the location of N–S cross-section is 3.3% (4.5 m). It can be concluded that there is an important difference in FGL geometry between the 2D and 3D models. The former actually represents an infinitely long (perpendicular to the cross-section) island, whereas the latter is semi-circular. The real 3D behavior of groundwater flow and solute transport therefore makes 3D simulation inevitable for most practical applications.

Obviously, the drawback of 3D simulations is its high computational burden for real and large-scale cases (Voss and Provost, 2010). It is worth noting that for instance, a steady-state model of ALS0 scenario requires approximately 6 to 10 min CPU time with 2.2 GHz processor to simulate 2D cross-sections, while the 3D simulation takes 19 min. The 3D model, considered in this study is relatively a coarse mesh for some of the flow processes such as unsaturated zone flow. Refining this discretization from 500 m to 100 m on the horizontal plane and the number of elements from 18,000 to 479,650 elements, tremendously increases the computation time to about 6000 min. Applying high-performance computational tools, efficient techniques such as parallel processing (e.g., Cheng et al., 2014; Zhang et al., 2014), local-grid refinement, or

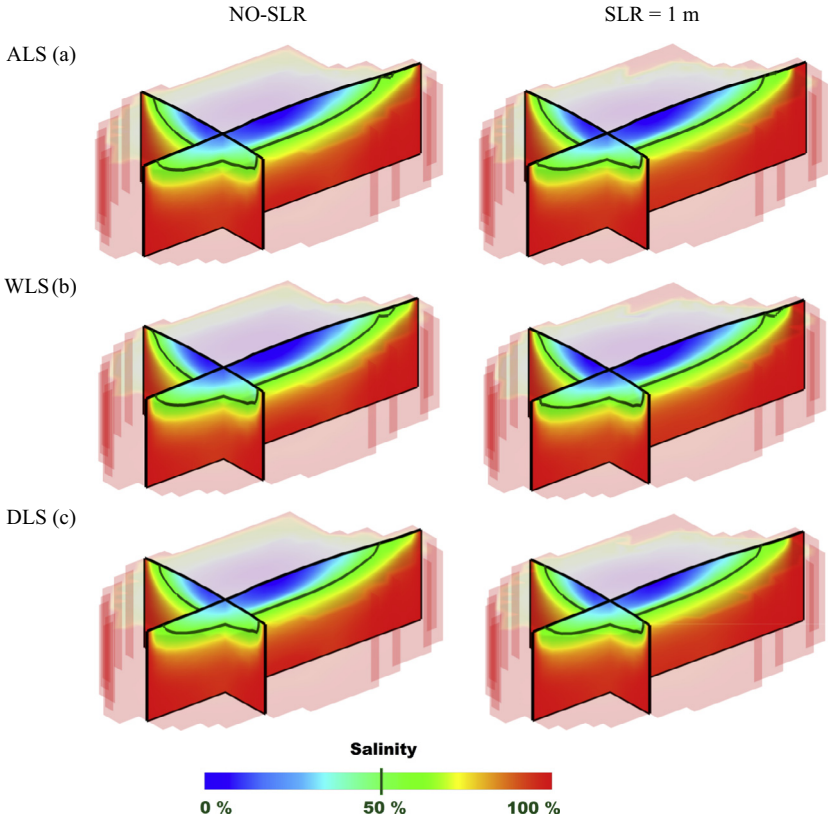

Fig. 11. Comparisons of the steady-state FGL under NO-SLR and SLR of 1 m condition using 3D modeling for (a) ALS scenarios, (b) WLS scenarios, and (c) DLS scenarios.

Table 5
The comparison of the maximum FGL thicknesses obtained from 2D and 3D models.

Scenario	N–S cross-section location		W–E cross-section location	
	Thickness (m) 3D model	Thickness (m) 2D model	Thickness (m) 3D model	Thickness (m) 2D model
ALS0	136.4	140.6	138.7	282.0
ALS1	129.4	126.2	133.3	256.0
WLS0	149.6	153.3	152.5	309.8
WLS1	143.5	138.7	147.9	281.0
DLS0	124.1	131.6	125.5	259.9
DLS1	119.5	116.2	122.3	236.2

artificial neural networks (ANNs) (e.g., Ataie-Ashtiani et al., 2014) are possible solutions for dealing with the challenges presented by realistic 3D conditions, models, and large-scale simulations.

7. Conclusions

There is a need to systematically and quantitatively assess various conceptualization choices in a unifying framework for real-case complex groundwater simulations of small islands. In this study, an arid-region island in the Persian Gulf is considered in this context as a real-world problem and the FGL behavior of Kish Island subject to climate change is studied. This study aims for the first time to understand how conceptual and numerical modeling choices influence FGL behavior on small islands and to better understand how and when various factors should be considered. We tested the influence of the aquifer layering and geometry, and also, the unsaturated zone conceptualization on simulation results. These results suggest that the assumption of the two-layer geology is important due to its significant influence on the FGL. On the other hand, the slope of the island's lateral boundary and its irregularities can often be neglected and simplified with a vertical face boundary below sea-level for the Kish Island case, due to the low hydraulic conductivity of base-layer. It is shown that instead of unsaturated zone modeling, we can remove this zone if the aquifer is a single-layer system or the thickness of the unsaturated zone is small compared to FGL thickness. Conversely, when a two-layer aquifer is considered, it is important to include an unsaturated zone modeling approach. 3D numerical models of the island are also developed based on the 2D simulations results to investigate the impacts of spatial dimensionality. The results confirm the necessity of the 3D simulations due to the 3D nature of boundary conditions of island, topography properties, irregularity of coastline, and irregular layering.

For simulating climate change in the Kish Island FGL system, predictions for changes in SLR and recharge rate are employed in the form of twelve scenarios. In these scenarios, the situation prior to SLR, SLR of 1 m, and 4 m are included considering the LSI impacts in combination with possible −15 to +20% changes in the mean net recharge rate of 20 mm/year. The steady-state results show that for the scenarios in which the impact of LSI is neglected, minor changes in the FGL position are observed. Consequently, LSI has a significant impact on the FGL of Kish Island, especially in low-topography sections. Furthermore, the results show that the significant changes on the existing FGL occur under recharge rate changes, suggesting recharge rate variations are a more influential factor in the FGL studies in comparison to the SLR magnitude, without LSI impacts. The simulations results emphasize the climate change impacts on the FGL are long-term and take hundreds years, or longer, to reach a new FGL equilibrium for the conditions studied here. The results of this work are expected to offer new guidance on appropriate conceptual and numerical modeling choices made when simulating FGL on small islands. This is important in support of evidence based modeling decision making.

Acknowledgments

The authors wish to thank Iran Kish Free Zone Organization for providing financial support and assistance for field data collections. The last two authors also appreciate the funding of National Centre for Groundwater Research and Training, a collaborative initiative of the Australian Research Council and the National Water Commission, Australia. The authors appreciate the comments of two anonymous reviewers, Associate Editor, and Editor-in-Chief Geoff Syme on this manuscript, which helped improve the final manuscript.

References

Abarca, E., Carrera, J., Sanchez-Vila, X., Voss, C.I., 2007. Quasi-horizontal circulation cells in 3D seawater intrusion. J. Hydrol. 339, 118–129.
Ataie-Ashtiani, B., Ketabchi, H., Rajabi, M.M., 2014. Optimal management of freshwater lens in a small island using surrogate models and evolutionary algorithms. J. Hydrol. Eng. 19 (2), 339–354.
Ataie-Ashtiani, B., Rajabi, M.M., Ketabchi, H., 2013a. Inverse modeling for freshwater lens in small islands: Kish Island, Persian Gulf. Hydrol. Process. 27, 2759–2773.
Ataie-Ashtiani, B., Werner, A.D., Simmons, C.T., Morgan, L.K., Lu, C., 2013b. How important is the impact of land-surface inundation on seawater intrusion caused by sea-level rise? Hydrogeol. J. 21 (7), 1673–1677.
Ataie-Ashtiani, B., 2010. Study of Optimum Groundwater Usage in Kish Island. Final Report. Iran Kish Free Zone Organization (KFZO).
Ataie-Ashtiani, B., Volker, R.E., Lockington, D.A., 1999. Tidal effects on seawater intrusion in unconfined aquifers. J. Hydrol. 216 (1–2), 17–31.
Ataie-Ashtiani, B., Volker, R.E., Lockington, D.A., 2001. Tidal effects on groundwater dynamics in unconfined aquifers. Hydrol. Process. 15 (4), 655–669.
Bailey, R.T., Jenson, J.W., Olsen, A.E., 2009. Numerical modeling of atoll island hydrogeology. Groundwater 47 (2), 184–196.
Banerjee, P., Singh, V.S., 2011. Optimization of pumping rate and recharge through numerical modeling with special reference to small coral island aquifer. Phys. Chem. Earth. 36 (16), 1363–1372.
Bricker, S.H., 2007. Impacts of Climate Change on Small Island Hydrogeology – A Literature Review. British Geological Survey Internal Report, OR/09/025. 28PP. Groundwater Science Programme, Open Report OR/09/025.
Chang, S.W., Clement, T.P., Simpson, M.J., Lee, K.K., 2011. Does sea-level rise have an impact on saltwater intrusion? Adv. Water. Resour. 34 (10), 1283–1291.
Cheng, T., Mo, Z., Shao, J., 2014. Accelerating groundwater flow simulation in MODFLOW using JASMIN-based parallel computing. Groundwater 52 (2), 194–205.
Doherty, J., 2005. PEST: Model Independent Parameter Estimation, user Manual, fifth ed. Watermark Numerical Computing.
Drees and Sommer, 2004. Kish Island Integrated Management Plan – Kish Island. Iran Kish Free Zone Organization, Kish Island, Iran.
Falkland, A., 1991. Hydrology and Water Resources of Small Islands: A Practical Guide. A contribution to the International Hydrological Programme. Paris, France: United Nations Educational, Scientific and Cultural Organization.
Flint, A.L., Flint, L.E., Hevesi, J.A., D'Agnese, F., Faunt, C., 2000. Estimation of regional recharge and travel time through the unsaturated zone in arid climates. Geophys. Monogr. Ser. 122, 115–128.
Gelhar, L.W., Welty, C., Rehfeldt, K.R., 1992. A critical review of data on field scale dispersion in aquifers. Water. Resour. Res. 28 (728), 1955–1974.
Ghassemi, F., Alam, K., Howard, K., 2000. Freshwater lenses and practical limitations of their three-dimensional simulation. Hydrogeol. J. 8, 521–537.
Hunt, R.J., Prudic, D.E., Walker, J.F., Anderson, M.P., 2008. Importance of unsaturated zone flow for simulating recharge in a humid climate. Groundwater 46 (4), 551–560.
International Panel on Climate Change (IPCC), 2007. Climate Change 2007: Impacts, Adaptation and Vulnerability. In: Parry, M.L., Canziani, O.F., Palutikof, J.P., van der Linden, P.J., Hanson, C.E. (Eds.). Contribution of Working Group II to the Fourth Assessment Report of the Intergovernmental Panel on Climate Change. Cambridge: Cambridge University Press.
International Panel on Climate Change (IPCC), 2013. Climate Change 2013: The Physical Science Basis. Working Group 1 Contribution to the Fifth Assessment Report of the International Panel on Climate Change. Cambridge, New York.
Ketabchi, H., Mahmoodzadeh, D., Ataie-Ashtiani, B., Werner, A.D., Simmons, C.T., 2014. Sea-level rise impact on fresh groundwater lenses in two-layer small islands. Hydrol. Process. http://dx.doi.org/10.1002/hyp.10059/hyp.0187.
Kish Free Zone Organization (KFZO), 2006. General Annual Reports. Kish Island, Iran.
Kopsiaftis, G., Mantoglou, A., Giannoulopoulos, P., 2009. Variable density coastal aquifer models with application to an aquifer on Thira Island. Desalination 237, 65–80.
Masterson, J.P., Garabedian, S.P., 2007. Effects of sea-level rise on groundwater flow in a coastal aquifer system. Groundwater 45 (2), 209–217.
Mehta, S., Fryar, A.E., Brady, R.M., Morin, R.H., 2000. Modeling regional salinization of the Ogallala aquifer, Southern High Plains, TX, USA. J. Hydrol. 238 (1), 44–64.
Melloul, A., Collin, M., 2006. Hydrogeological changes in coastal aquifers due to sea level rise. Ocean. Coast. Manage. 49, 281–297.
Middlemis, H., 2000. Groundwater Flow Modeling Guidline. Marray-Darling Basin Commision-Australia, Aquiterra Consulting Pty Ltd.
Michael, H.A., Russoniello, C.J., Byron, L.A., 2013. Global assessment of vulnerability to sea-level rise in topography-limited and recharge-limited coastal groundwater systems. Water. Resour. Res. 49 (4), 2228–2240.
Nadim, F., Bagtzoglou, A.C., Iranmahboob, J., 2008. Coastal management in the Persian Gulf region within the framework of the ROPME programme of action. Ocean. Coast. Manage. 51 (7), 556–565.
Oude Essink, G.H.P., Van Baaren, E.S., De Louw, P.G.B., 2010. Effects of climate change on coastal groundwater systems: a modeling study in the Netherlands. Water. Resour. Res. 46 (null), W00F04.
Payne, D.F., 2010. Effects of climate change on saltwater intrusion at Hilton Head Island, SC. U.S.A. SWIM21 – 21st Salt Water Intrusion Meeting, Azores, Portugal, pp. 293–296.

Praveena, S.M., Abdullah, M.H., Aris, A.Z., Mokhtar, M., Bidin, K., 2011. Numerical simulation of seawater intrusion in Manukan Island, East Malaysia. J. Model. Manage. 6 (3), 317–333.
Preusser, F., Radtke, U., Fontugne, M., Haghipour, A., Hilgers, A., Kasper, H.U., Nazari, H., Pirazzoli, P.A., 2003. ESR dating of raised coral reefs from Kish Island, Persian Gulf. Quaternary Sci. Rev. 22 (10), 1317–1322.
Rajabi, M.M., Ataie-Ashtiani, B., 2014. Sampling efficiency in Monte Carlo based uncertainty propagation strategies: application in seawater intrusion simulations. Adv. Water. Resour. 67, 46–64.
Rozell, D.J., Wong, T., 2010. Effects of climate change on groundwater resources at Shelter Island, New York State, USA. Hydrogeol. J. 18 (7), 1657–1665.
Schneider, J.C., Kruse, S.E., 2006. Assessing selected natural and anthropogenic impacts on freshwater lens morphology on small barrier Islands: Dog Island and St. George Island, Florida, USA. Hydrogeol. J. 14 (1–2), 131–145.
Sefelnasr, A., Sherif, M., 2014. Impacts of seawater rise on seawater intrusion in the Nile delta aquifer, Egypt. Groundwater 52 (2), 264–276.
Shamrukh, M., Corapcioglu, M.Y., Hassona, F.A.A., 2001. Modeling the effect of chemical fertilizers on ground water quality in the Nile Valley aquifer, Egypt. Groundwater 39, 59–67.
Stoeckl, L., Houben, G., 2012. Flow dynamics and age stratification of freshwater lenses: experiments and modeling. J. Hydrol. 458, 9–15.
Sulzbacher, H., Wiederhold, H., Siemon, B., Grinat, M., Igel, J., Burschil, T., Gunther, T., Hinsby, K., 2012. Numerical modeling of climate change impacts on freshwater lenses on the North Sea Island of Borkum using hydrological and geophysical methods. Hydrol. Earth. Syst. Sci. 16, 3621–3643.
Underwood, M.R., Peterson, F.L., Voss, C.I., 1992. Groundwater lens dynamics of atoll islands. Water. Resour. Res. 28 (11), 2889–2902.
Van Genuchten, M.T., 1980. A closed-form equation for predicting the hydraulic conductivity of unsaturated soils. Soil. Sci. Soc. Am. J. 44 (5), 892–898.
Vermeer, M., Rahmstorf, S., 2009. Global sea level linked to global temperature. Proc. Nat. Acad. Sci. USA 106 (51), 21527–21532.
Voss, C.I., Provost, A.M., 2010. SUTRA: A model for saturated-unsaturated, variable-density groundwater flow with solute or energy transport. USGS Water-Resources Investigations Report, 02-4231, U.S. Geological Survey, Reston, VA.
Voss, C.I., Souza, W.R., 1987. Variable density flow and solute transport simulation of regional aquifers containing a narrow freshwater-seawater mixing zone. Water. Resour. Res. 23 (10), 1851–1866.
Watson, A., Werner, A.D., Simmons, C.T., 2010. Transience of seawater intrusion in response to sea level rise. Water. Resour. Res. 46 (12), W12533, 10 pp..
Webb, M.D., Howard, K.W., 2011. Modeling the transient response of saline intrusion to rising sea-levels. Groundwater 49 (4), 560–569.
Werner, A.D., Simmons, C.T., 2009. Impact of sea-level rise on seawater intrusion in coastal aquifers. Groundwater 47 (2), 197–204.
Werner, A.D., Gallagher, M.R., 2006. Characterization of seawater intrusion in the Pioneer Valley, Australia using hydrochemistry and three-dimensional numerical modeling. Hydrogeol. J. 14 (8), 1452–1469.
White, I., Falkland, T., 2010. Management of freshwater lenses on small Pacific islands. Hydrogeol. J. 18 (1), 227–246.
Xu, M., Eckstein, Y., 1995. Use of weighted least-squares method in evaluation of the relationship between dispersivity and field scale. Groundwater 33, 905–908.
Yakirevich, A., Melloul, A., Sorek, S., Shaath, S., Borisov, V., 1998. Simulation of seawater intrusion into the Khan Yunis area of the Gaza Strip coastal aquifer. Hydrogeol. J. 6 (4), 549–559.
Zhang, S., Xia, Z., Yuan, R., Jiang, X., 2014. Parallel computation of a dam-break flow model using OpenMP on a multi-core computer. J. Hydrol. 512, 126–133.